Integrated modeling for determining launch survival and limitations of actuated, lightweight mirrors

Citation: Cohan, Lucy E., and David W. Miller. "Integrated modeling for determining launch survival and limitations of actuated lightweight mirrors." Space Telescopes and Instrumentation 2008: Optical, Infrared, and Millimeter. Ed. Jacobus M. Oschmann et al. Marseille, France: SPIE, 2008. 70102I-12. © 2008 SPIE--The International Society for Optical Engineering

As Published: http://dx.doi.org/10.1117/12.789079

Publisher: The International Society for Optical Engineering

Persistent URL: http://hdl.handle.net/1721.1/52724

Version: Final published version: final published article, as it appeared in a journal, conference proceedings, or other formally published context

Integrated Modeling for Determining Launch Survival and Limitations of Actuated, Lightweight Mirrors

Lucy E. Cohan and David W. Miller

Massachusetts Institute of Technology, 77 Massachusetts Ave, Cambridge, MA

ABSTRACT

The future of space telescopes lies in large, lightweight, segmented aperture systems. Segmented apertures eliminate manufacturability and launch vehicle fairing diameter as apertures size constraints. Low areal density, actuated segments allow the systems to meet both launch mass restrictions and on-orbit wavefront error requirements. These systems, with silicon carbide as a leading material, have great potential for increasing the productivity, affordability, and manufacturability of future space-based optical systems.

Thus far, progress has been made on the manufacturing, sensing, actuation, and on-orbit control of such systems. However, relatively little attention has been paid to the harsh environment of launch. The launch environment may dominate aspects of the design of the mirror segments, with survivability requirements eliminating many potentially good designs. Integrated modeling of a mirror segment can help identify trends in mirror geometries that maximize launch performance, ensuring survivability without drastically over designing the mirror. A finite element model of a single, ribbed, actuated, silicon carbide mirror segment is created, and is used to develop a dynamic, state-space model, with launch load spectra as disturbance inputs, and mirror stresses as performance outputs. The parametric nature of this model allows analysis of many geometrically different mirror segments, helping to identify key parameters for launch survival. The modeling method described herein will enable identification of the design decisions that are dominated by launch, and will allow for development of launch-load alleviation techniques to further push the areal density boundaries in support of the creation of larger and lighter mirrors than previously possible.

Keywords: Space Telescope, Integrated Modeling, Launch Survival, Lightweight Mirrors

1. INTRODUCTION

In pursuit of further scientific advancement, future space telescopes are moving toward larger apertures.[1,2] However, larger apertures come with many challenges, such as launch mass, volume, and cost. Therefore, there is a push for new mirror technologies to overcome these difficulties. One such option is to use segmented apertures with actuated silicon carbide mirror segments. Segmented apertures can be deployed, eliminating the launch fairing diameter as the aperture size constraint. Also, segmented apertures are made of multiple smaller mirror segments, many of which are identical. Therefore, a replication process can be used in the manufacturing, decreasing the immense costs associated with manufacturing very large mirrors. Additionally, silicon carbide mirrors can be manufactured to low areal densities, decreasing the large masses associated with the primary mirror, while the actuation and active optics allows these systems with lower areal densities to meet the desired on-orbit performance requirements. Therefore, actuated, silicon carbide mirrors provide a promising path for future space telescopes.[3,4]

While they have a great potential for success, these mirrors are not without issues and concerns that need attention. One such concern is in the reaction of the mirrors to the harsh launch environment. As areal densities are lowered, one must be sure that the brittle silicon carbide mirror will still survive launch. If launch survival materializes as a major issue, various active and passive techniques could be utilized to expand the range of design possibilities that survive the launch. With this in mind, a parametric model of a mirror segment is developed to create a dynamic model of the mirror exposed to the launch environment. This allows for analysis of various

Further author information: (Send correspondence to Lucy E. Cohan)
L. Cohan: E-mail: lcohan@mit.edu, Telephone: 1 617 253 8364
D. Miller: E-mail: millerd@mit.edu, Telephone: 1 617 253 3288

Space Telescopes and Instrumentation 2008: Optical, Infrared, and Millimeter,
edited by Jacobus M. Oschmann, Jr., Mattheus W. M. de Graauw, Howard A. MacEwen,
Proc. of SPIE Vol. 7010, 70102I, (2008) · 0277-786X/08/$18 · doi: 10.1117/12.789079

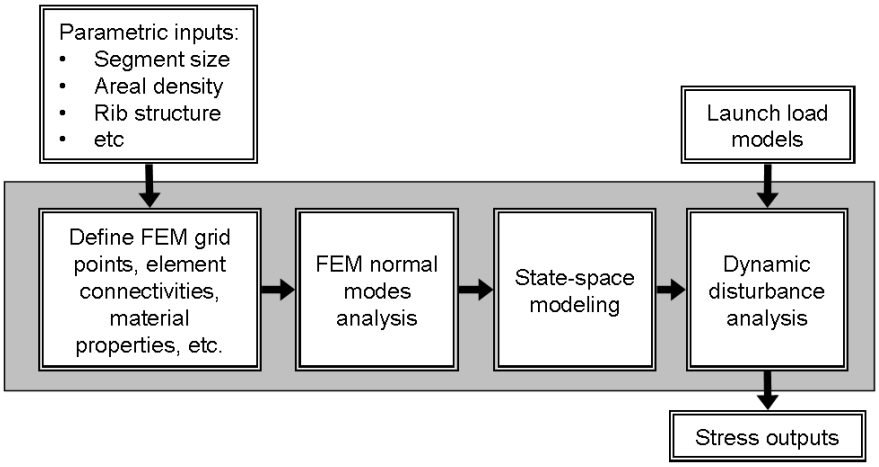

Figure 1. Parametric, integrated modeling environment

mirror designs during launch, and is also conducive to adding passive or active damping to expand the design possibilities.

This paper focuses on a modeling methodology that can be utilized for design and optimization of mirrors subjected to launch loads. This approach uses parametric, integrated modeling to analyze the stresses induced by launch, and allows one to easily change the mirror geometry and design. First, the parametric modeling philosophy is discussed. Then the different aspects of the model, and how they can be used for future design and analysis are described.

2. PARAMETRIC MODELING

Because of the novelty of actuated, silicon carbide mirror segments, the design intuition that is available for traditional glass mirrors is lacking. Therefore, general design "rules of thumb" are unavailable for such mirrors. Hence, it is useful to explore a large trade space of mirror designs, since the optimal design is not known a priori. One way to accomplish this task is to use parametric modeling techniques.[5] Here, all design variables are parameterized in a separate input file, and many different mirror designs can be generated by simply changing the inputs. The parameterized inputs include, but are not limited to: segment size, areal density, radius of curvature, rib structure, rib aspect ratio, damping coefficient, and material properties. The parameterized inputs are used to automatically create the necessary grid points and elements for a finite element model (FEM). A finite element normal modes analysis is run, and the results are used to create a state-space model. Launch load models are also imported and combined with the state-space model into a dynamic disturbance analysis, with element stress as a performance output. An overview of the parametric, integrated modeling scheme considered in this paper can be seen in Figure 1.

This modeling method helps to determine the stresses across the mirror during the launch process. The benefit of this technique is that it allows one to very quickly analyze a variety of mirror designs and compare the resulting performance. Also, the dynamic, state-space, MATLAB-based modeling allows for the easy future addition of control and damping. The remainder of this paper describes each of the model components in greater detail, and the process by which results can be obtained from such a model.

3. STRUCTURAL FINITE ELEMENT MODEL

The finite element model considered in this paper is of a single mirror segment, an example of which can be seen in Figure 2. It is rib-stiffened with silicon carbide material properties. There are surface-parallel electrostrictive actuators embedded in the ribs, allowing for actuation of the mirror. These actuators can also be seen in Figure 2, represented as bars. The curvature, areal density, number of ribs, rib aspect ratio, and percent of the mass in

the facesheet are all variable. The mirror is made up of 2-dimensional shell elements; the surface is triangular elements and the ribs are quadrilateral elements.

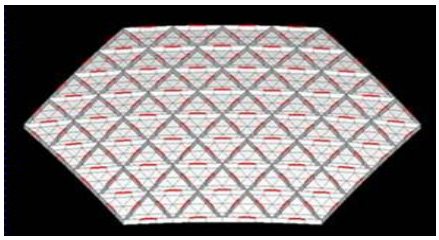

Figure 2. Mirror FEM Model

The mirror constraint configuration can be seen in Figure 3. In this configuration, the mirror is connected to three bipod mounts. The connection between the rigid triangle and the mirror mimics that of a kinematic bipod flexure that helps to mitigate the transference of disturbance energy from the structure to the aperture. They constrain motion in the vertical (z) and circumferential (θ) directions. There is a soft spring connecting the radial (r) and rotational degrees of freedom which connect, but do not rigidly constrain, the motion in these degrees of freedom. Specifically, the soft degrees of freedom of the bipods have very low stiffness, so deformation of the structure creates rigid body motion of the mirror segment, but still constrains all six degrees of freedom. The bipod connections to the mirror are created with a load-spreading technique to eliminate a large stress concentration resulting from a single node connection. This method connects the bipod to seven points on the mirror (the center point at the rib intersection, and the first node outwards on each rib), as seen in Figure 4, eliminating the stress concentration caused by connecting at a single node.

The three bipods are connected to a rigid backstructure element, and the central point of the backstructure is then connected through a soft spring to a point that is constrained to space in all six degrees of freedom. This eliminates the six rigid body modes. The vibrational launch loads are then applied to the central point of the backstructure. The spring between the backstructure and the constraint point has a frequency that is below the frequency range of the disturbance, so it eliminates the rigid body modes without affecting the performance.

A number of simplifying assumptions were made for the finite element model. The first is that this is an on-axis segment. The real mirrors would be off-axis since they are part of a larger aperture. However, symmetry can be exploited in an on-axis segment, and this assumption can easily be lifted for the final designs. Second, the flexible backstructure is eliminated, and the bipods are connected to a rigid element. This method preserves the same modal frequencies as if the system was constrained in the z and θ directions at the three bipod points directly. However, it eliminates the additional modeling complexity associated with the structure. Finally, there is a plane stress assumption because the FEM is made up of two-dimensional shell elements. These simplifications should not have a significant effect on the final results. However, they help to keep the model simple enough to use for trade space exploration and rapid design generation. The FEM described above is defined within MATLAB, and the resulting FEA is solved using NASTRAN. The results are then brought into MATLAB, where the model process continues.

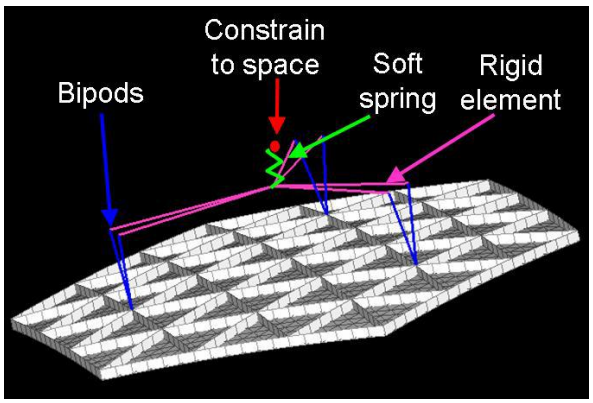

Figure 3. Mirror FEM constraint configuration

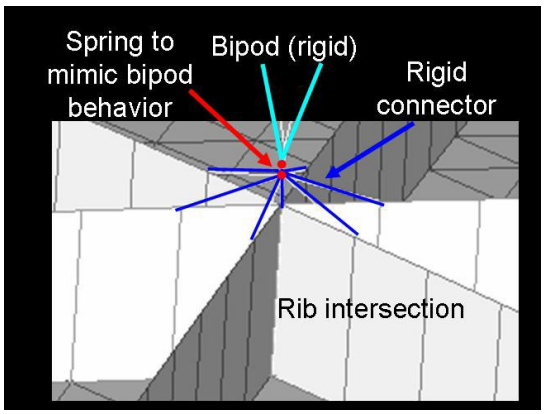

Figure 4. Load spreading configuration

4. STATE-SPACE MODEL

The finite element solver combines the defined grid points, elements, and material properties into mass and stiffness matrices as follows:

$$M\ddot{\eta} + K\eta = 0 \tag{1}$$

where M is the mass matrix, K is the stiffness matrix, and η are the nodal degrees of freedom. NASTRAN then solves this eigenvalue problem for the natural frequencies and mode shapes of the system.

$$\left(K - \Omega^2 M\right)\Phi = 0 \tag{2}$$

where Ω are the modal frequencies and Φ are the mode shapes of the system. The frequencies and mode shapes are then combined to form the dynamics (A matrix) of a state-space model of the system.

$$\begin{aligned} \begin{bmatrix} \dot{q} \\ \ddot{q} \end{bmatrix} &= \begin{bmatrix} 0 & I \\ -\Omega^2 & -2\zeta\Omega \end{bmatrix} \begin{bmatrix} q \\ \dot{q} \end{bmatrix} + B_w w \\ z &= C_z \begin{bmatrix} q \\ \dot{q} \end{bmatrix} \end{aligned} \tag{3}$$

where q are the modal degrees of freedom, w is the disturbance input, B_w defines the way in which the disturbances are input into the system, z are the performance outputs, and C_z relates the performance outputs to the states. The FEM defines the dynamics of the system (Ω), leaving the input and output matrices (B_w and C_z) to be defined. In this particular problem, the desired performance output is stress, and the desired input is launch load disturbance power spectral densities (PSDs). The following two sections describe the method by which the desired input and output matrices are obtained.

4.1 Mirror Model Outputs

In analyzing the mirror's response to launch, stress is the relevant output of the integrated, state-space model. The typical outputs from a model such as the one in Equation 3 are linear combinations of displacements, rates, or accelerations of nodes in the FEM. For this problem, those types of outputs need to be transformed into stress. In order to accomplish this, finite element theory will be used. The overarching strategy is as follows:

1. Start with the nodal displacements from each node in the desired element.
2. Transform the three-dimensional nodal displacements into two-dimensional displacements in the plane of the element (projection).
3. Multiply by a strain transformation matrix.
4. Use Hooke's law to obtain stress.

The key steps in this method are subsequently described.

4.1.1 Projection Transformation

For each element analyzed, there are either three (triangular elements in the facesheet) or four (quadrilateral elements in the ribs) grid points. The objective of this step is to find a transformation matrix to project displacements into the plane of the element, and to find the two-dimensional grid points (with a constant third degree of freedom across the element). For each element, three grid points are used. These grid points can be defined as points a, b, and c. Next, the vectors between the points, ab and bc, can be easily computed. Then:

$$\begin{aligned} u &= ab \\ w &= ab \times bc \\ v &= w \times u \end{aligned} \tag{4}$$

The u, v, and w vectors are then normalized. The three vectors (1 x 3) are then combined:

$$M_{full} = \begin{bmatrix} u \\ v \\ w \end{bmatrix} \tag{5}$$

Finally, to eliminate the (now equal) out-of-plane degree of freedom, the projection matrix in equation 5 is premultiplied as follows:

$$M = \begin{bmatrix} 1 & 0 & 0 \\ 0 & 1 & 0 \end{bmatrix} M_{full} \tag{6}$$

The resulting matrix, M, is now a 2 by 3 matrix that will transform displacements from general three dimensional space into two-dimensional displacements in the plane of the relevant element. Each element has its own projection matrix. Therefore, they must be combined with the displacement outputs to obtain the desired displacements for each element.

4.1.2 Strain Transformation Matrix

The strain transformation matrix is taken from finite element theory.[6] It uses interpolation functions to determine the strains over an element. There are two different formations: one for triangular elements and one for quadrilateral elements. The triangular element formulation gives a constant strain over the element, while the quadrilateral element case computes strain as a function of internal coordinates, resulting in a strain (and stress) distribution over the element. The two formulations are very similar, thus, only the slightly more complex case of the quadrilateral elements is presented below. The overarching goal is to find a matrix (B) which relates the strain in an element to the nodal displacements of the corner grid points:

$$\epsilon = \begin{bmatrix} \epsilon_{xx} \\ \epsilon_{yy} \\ 2\epsilon_{xy} \end{bmatrix} = \begin{bmatrix} \frac{\partial u_x}{\partial x} \\ \frac{\partial u_y}{\partial y} \\ \frac{\partial u_x}{\partial y} + \frac{\partial u_y}{\partial x} \end{bmatrix} = B\hat{u} \tag{7}$$

where ϵ is strain, u is displacement, B is the strain transformation matrix, and x and y are the in-plane degrees of freedom for each element.

To calculate the displacements and strains, displacement and strain interpolation matrices are defined respectively as follows:

$$H = \begin{bmatrix} h_1 & 0 & h_2 & 0 & h_3 & 0 & h_4 & 0 \\ 0 & h_1 & 0 & h_2 & 0 & h_3 & 0 & h_4 \end{bmatrix} \tag{8a}$$

$$B = \begin{bmatrix} h_{1,x} & 0 & h_{2,x} & 0 & h_{3,x} & 0 & h_{4,x} & 0 \\ 0 & h_{1,y} & 0 & h_{2,y} & 0 & h_{3,y} & 0 & h_{4,y} \\ h_{1,y} & h_{1,x} & h_{2,y} & h_{2,x} & h_{3,y} & h_{3,x} & h_{4,y} & h_{4,x} \end{bmatrix} \tag{8b}$$

where $h_{i,x}$ is the x-derivative of the interpolation function, h_i. The interpolation functions for the quadrilateral elements are defined as:

$$\begin{aligned} h_1 &= 0.25(1+r)(1+s) \\ h_2 &= 0.25(1-r)(1+s) \\ h_3 &= 0.25(1-r)(1-s) \\ h_4 &= 0.25(1+r)(1-s) \end{aligned} \tag{9}$$

where r and s are internal coordinates. These interpolation functions sum to one, as required. They are also equal to 1 at the given node, and 0 at the other nodes, where node 1 is at $(r,s) = (1,1)$, node 2 is at $(r,s) = (-1,1)$, node 3 is at $(r,s) = (-1,-1)$, and node 4 is at $(r,s) = (1,-1)$.

These interpolation functions define the H matrix. To determine the B matrix, the derivatives with respect to x and y must be computed. By the chain rule, one can obtain:

$$\begin{bmatrix} \frac{\partial h_1}{\partial x} & \frac{\partial h_2}{\partial x} & \frac{\partial h_3}{\partial x} & \frac{\partial h_4}{\partial x} \\ \frac{\partial h_1}{\partial y} & \frac{\partial h_2}{\partial y} & \frac{\partial h_3}{\partial y} & \frac{\partial h_4}{\partial y} \end{bmatrix} = \begin{bmatrix} \frac{\partial r}{\partial x} & \frac{\partial s}{\partial x} \\ \frac{\partial r}{\partial y} & \frac{\partial s}{\partial y} \end{bmatrix} \begin{bmatrix} \frac{\partial h_1}{\partial r} & \frac{\partial h_2}{\partial r} & \frac{\partial h_3}{\partial r} & \frac{\partial h_4}{\partial r} \\ \frac{\partial h_1}{\partial s} & \frac{\partial h_2}{\partial s} & \frac{\partial h_3}{\partial s} & \frac{\partial h_4}{\partial s} \end{bmatrix} \tag{10}$$

and the Jacobian is defined as:

$$\begin{aligned} J &= \begin{bmatrix} \frac{\partial x}{\partial r} & \frac{\partial x}{\partial s} \\ \frac{\partial y}{\partial r} & \frac{\partial y}{\partial s} \end{bmatrix} \\ &= 0.25 \begin{bmatrix} (1+s) & -(1+s) & -(1-s) & (1-s) \\ (1+r) & (1-r) & -(1-r) & -(1+r) \end{bmatrix} \begin{bmatrix} x_1 & y_1 \\ x_2 & y_2 \\ x_3 & y_3 \\ x_4 & y_4 \end{bmatrix} \\ &= 0.25 \begin{bmatrix} (x_1-x_2)(1+s)+(x_4-x_3)(1-s) & (y_1-y_2)(1+s)+(y_4-y_3)(1-s) \\ (x_1-x_4)(1+r)+(x_2-x_3)(1-r) & (y_1-y_4)(1+r)+(y_2-y_3)(1-r) \end{bmatrix} \end{aligned} \tag{11}$$

J^{-1} can then be calculated as:

$$J^{-1} = \frac{0.25}{det(J)} \begin{bmatrix} (y_1-y_4)(1+r)+(y_2-y_3)(1-r) & (y_2-y_1)(1+s)+(y_3-y_4)(1-s) \\ (x_4-x_1)(1+r)+(x_3-x_2)(1-r) & (x_1-x_2)(1+s)+(x_4-x_3)(1-s) \end{bmatrix} \tag{12}$$

Finally, the matrix of derivatives can be calculated from:

$$\begin{bmatrix} h_{1,x} & h_{2,x} & h_{3,x} & h_{4,x} \\ h_{1,y} & h_{2,y} & h_{3,y} & h_{4,y} \end{bmatrix} = 0.25 J^{-1} \begin{bmatrix} (1+s) & -(1+s) & -(1-s) & (1-s) \\ (1+r) & (1-r) & -(1-r) & -(1+r) \end{bmatrix} \tag{13}$$

Equation 12 can be substituted into Equation 13, and the values from the matrix in Equation 13 can be substituted into their appropriate places in Equation 8 to obtain the strain interpolation matrix for the quadrilateral elements. This can be multiplied by the nodal displacements to obtain the strain across the element. This methodology provides a way to transform the displacements of the nodes of an element, which are easy to compute, into a strain distribution across the element (in terms of the internal coordinates, r and s).

4.2 Stress Transformation

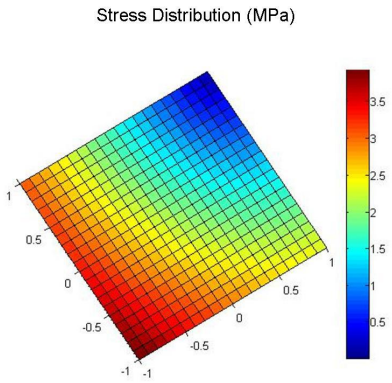

Figure 5. Stress distribution as a function of internal coordinates, r and s

Once the strain matrices are constructed, Hooke's law can be used to relate the desired stress to the strain. Hooke's law for plane stress is:[7]

$$\begin{bmatrix} \sigma_x \\ \sigma_y \\ \sigma_{xy} \end{bmatrix} = \frac{E}{1-\nu^2} \begin{bmatrix} 1 & \nu & 0 \\ \nu & 1 & 0 \\ 0 & 0 & \frac{1-\nu}{2} \end{bmatrix} \begin{bmatrix} \epsilon_x \\ \epsilon_y \\ 2\epsilon_{xy} \end{bmatrix} \tag{14}$$

The Hooke's law matrix can be multiplied by the strain transformation matrix to get the stress in elemental $x-y$ coordinates from nodal displacements.

These steps combine to allow for stress distribution outputs from a state-space model constructed using normal modes analysis. The nodal displacement outputs of the element are transformed to obtain a stress distribution in the mirror that can be used for launch load analysis. An example of the types of stress distributions over an element that are computed can be found in Figure 5.

4.3 Mirror Model Launch Disturbance Input

With the dynamics and the output matrices defined, the remaining component of the model in Equation 3 is the input matrix (B_w). The desired analysis is a dynamic disturbance analysis, described in Section 6. Therefore, the inputs to the model will be in terms of power spectral densities. The two sources of launch disturbances currently under consideration are vibrations and acoustics. Other disturbances such as shock events will be considered at a later time. The inputs to the mirror model for each of the two considered disturbances will be described in the following section.

4.3.1 Vibration Input

In the case of launch vibrations, the disturbance input is typically provided in terms of an acceleration spectral density. The most natural type of input to the model is a force or moment spectral density. Thus, these typical inputs must be modified to account for the alternate input type. This is treated as a base acceleration problem, similar to the types of analysis done for earthquakes.[8,9] A simple derivation of ground acceleration, based on Figure 6, is presented below.

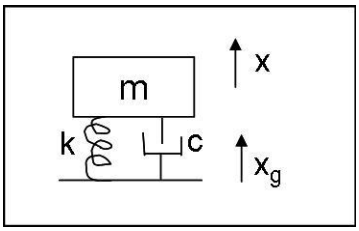

Figure 6. Diagram of base acceleration

$$M\ddot{x} + C\left(\dot{x} - \dot{x}_g\right) + K\left(x - x_g\right) = 0 \tag{15a}$$
$$y = x - x_g \tag{15b}$$
$$\dot{y} = \dot{x} - \dot{x}_g \tag{15c}$$
$$\ddot{y} = \ddot{x} - \ddot{x}_g \tag{15d}$$
$$M\left(\ddot{y} + \ddot{x}_g\right) + C\dot{y} + Ky = 0 \tag{15e}$$
$$M\ddot{y} + C\dot{y} + Ky = -M\ddot{x}_g \tag{15f}$$

where M is the mass matrix, C is the damping matrix, K is the stiffness matrix, y is a relative coordinate, and x_g is the base acceleration. The typical normal modes analysis can follow:

$$\Phi^T M \Phi \ddot{q} + \Phi^T C \Phi \dot{q} + \Phi^t K \Phi q = -\Phi^T M \ddot{x}_g \tag{16a}$$

$$\ddot{q} + 2\zeta\Omega\dot{q} + \Omega^2 q = -\Phi^T M \ddot{x}_g \tag{16b}$$

where Φ is the matrix of mass-normalized mode shapes, Ω is the matrix of modal frequencies, ζ is the damping coefficient, and q are the modal degrees of freedom. When put into the familiar state-space matrix form, the equations in 16 become:

$$\begin{bmatrix} \dot{q} \\ \ddot{q} \end{bmatrix} = \begin{bmatrix} 0 & I \\ -\Omega^2 & -2\zeta\Omega \end{bmatrix} \begin{bmatrix} q \\ \dot{q} \end{bmatrix} + \begin{bmatrix} 0 \\ -\Phi^T M F \end{bmatrix} \ddot{x}_g \tag{17}$$

Noting that the mode shape matrix, Φ, is mass normalized:

$$\Phi^T M = \Phi^T \left(\Phi^{-T} \Phi^{-1} \right) = \Phi^{-1} \tag{18}$$

where Φ^{-1} is a pseudo inverse. This simplifies equation 17 to include only the mode shape matrix, which is much easier to obtain than the very large mass matrix. Additionally, that term is post-multiplied by another matrix (F) that points to the specific degrees of freedom into which the launch loads are applied, since the actual system has many more degrees of freedom than the simple system in pictured Figure 6.

This method transforms the appropriate portions of the B_w matrix in the model to accept an acceleration PSD as an equivalent force PSD. Then, typical state-space techniques can be applied.

4.3.2 Acoustic Load Input

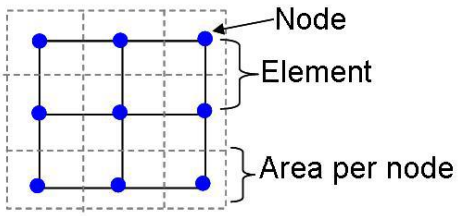

Figure 7. Force application of a pressure input

The second source of disturbances presently considered is acoustic loading. Acoustic loads are generally applied as pressures. In this type of model, a pressure is difficult to apply directly. Therefore, a pressure approximation is used. An equivalent force is applied to every node on the mirror surface. The pressure input is then scaled by the approximate area per node, where the surface area is divided up into small segments centered around the nodes, as seen in the diagram in Figure 7.

The force application direction is normal to the mirror surface. This has been found to be the worst case angle. The critical angle for acoustic pressure waves is that where the wave number of the acoustic wave projected on the mirror surface equals that of the structural bending mode.

$$k_{str} = k_{ac} sin\left(\theta_{cr}\right) \tag{19}$$

where k_{str} is the structural wave number, k_{ac} is the acoustic wave number, and θ_{cr} is the critical angle. The structural and acoustic wave numbers can be described in terms of basic quantities as follows:

$$k_{ac}^2 = \alpha^2 \omega^2 \qquad \alpha^2 = \frac{1}{\gamma R T} \tag{20a}$$

$$k_{str}^4 = \beta^4 \omega^2 \qquad \beta^4 = \frac{\rho A}{E I} \tag{20b}$$

where ω is frequency, $\frac{1}{\alpha}$ is the speed of sound, γ is the adiabatic index, R is the gas constant, T is temperature, ρ is density, A is area, E is Young's modulus, and I is the area moment of inertia. Equations 19 and 20 can be combined to yield:

$$\beta\sqrt{\omega} = \alpha\omega sin\left(\theta_{cr}\right) \tag{21a}$$

$$sin\left(\theta_{cr}\right) = \frac{\beta}{\alpha\sqrt{\omega}} \tag{21b}$$

The maximum of $sin\left(\theta_{cr}\right)$ is 1, so the cut-off frequency for critical angles (ω_c) is:

$$1 = \frac{\beta}{\alpha\sqrt{\omega}} \tag{22a}$$

$$\omega_c = \left(\frac{\beta}{\alpha}\right)^2 \tag{22b}$$

For simplicity, the mirror is approximated as a circular plate, and the speed of sound is calculated at sea-level. The numerical values for a typical mirror can be seen in Table 1. This yields a frequency cut-off of 211.6 rad/s, or approximately 33 Hz. The critical angle for all frequencies above ω_c is surface normal.

Table 1. Numerical values used to calculate the frequency cut-off for critical angles

ρ	3200	$\frac{kg}{m^2}$
A	0.866	m^2
E	375 10^9	Pa
I	0.0871	m^4
β	0.0171	$\frac{\sqrt{s}}{m}$
α	0.0029	$\frac{s}{m}$

As will be seen in Section 5.2, the acoustic disturbance spectrum utilized begins at a frequency of approximately 20 Hz. Therefore, for the purposes of this analysis, the worst-case angle is assumed to be surface normal for all frequencies, and the forces used to approximate the pressure waves are all applied normal to the mirror surface.

The appropriate nodes are selected for the B_w matrix to account for the required normal force on each node on the surface of the mirror. This portion of the matrix is then combined with the vibration inputs from Section 4.3.1 to form the entire B_w matrix. Now, all values in Equation 3 are defined, and appropriate launch disturbance spectra can be applied to the model.

5. LAUNCH LOAD MODEL

As described in Section 6, the analysis portion needs a spectral density function as a disturbance input. Therefore, an acceleration spectral density is defined for the vibrational disturbances, and a pressure spectral density is converted to a power spectral density for the acoustic input. These two disturbance spectra are described below.

5.1 Vibration Acceleration Spectral Density

There are many launch load vibration spectra available, but they differ by launch vehicle. The parametric nature of the model makes it east to change the disturbance spectra for whatever launch vehicle is applicable. Currently, the launch load spectrum being utilized can be seen in Figure 8. This is based on the qualification spectra for the space shuttle.[10,11]

The loading configuration must also be specified. While this is again a parametric input that is easily changed, the default configuration is shown in Figure 9. Here, the thrust axis is along the global x-axis, which indicates that the mirror segment is in a stowed configuration. This is expected to be the most likely case, but is easily alterable to see the effects of other configurations.

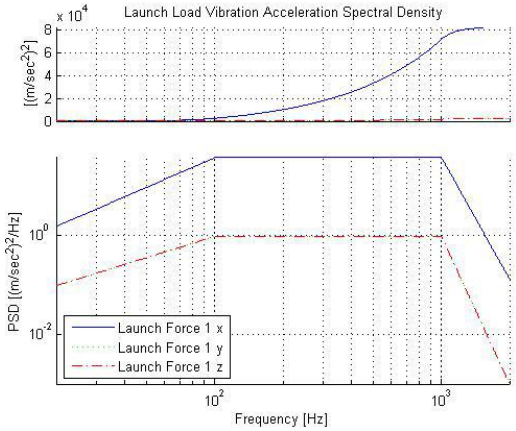

Figure 8. Launch acceleration PSD

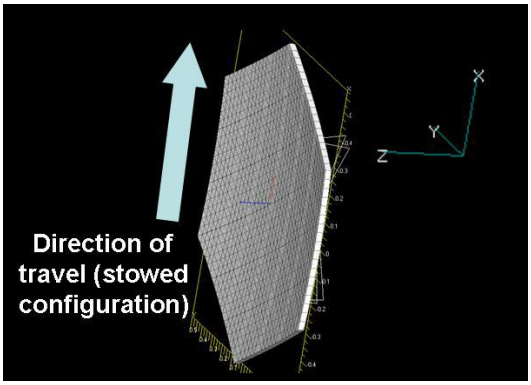

Figure 9. Launch force input configuration

5.2 Acoustic Disturbance Spectrum

The pressure spectral density is obtained from a sound pressure level chart. These are readily available, and the one currently in use can be seen in Figure 10.[12] This can be converted to the desired form and units through the following steps (for one-third octave bands):

$$P(f) = P_{ref} 10^{\frac{SPL(f)}{20}} \tag{23a}$$

$$\Delta_f(f) = \left(2^{1/6} - 2^{-1/6}\right) = 0.2316f \tag{23b}$$

$$PSD(f) = \frac{P(f)^2}{\Delta_f(f)} \tag{23c}$$

where P_{ref} is the reference pressure, $SPL(f)$ is the given sound pressure level curve (Figure 10), $\Delta_f(f)$ is the frequency band size, and $PSD(f)$ is the desired pressure spectral density (Figure 11). Using the force approximation described in Section 4.3.2, this disturbance spectrum can be used with the force inputs to the mirror model to determine stresses.

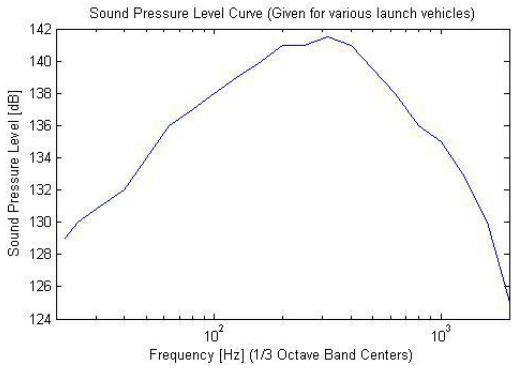

Figure 10. Sound Pressure Level

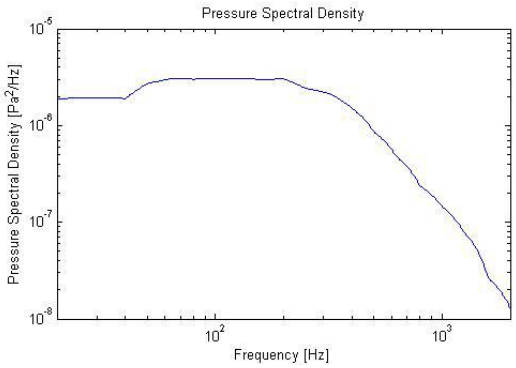

Figure 11. Pressure Spectral Density

6. DISTURBANCE ANALYSIS

With the state space model of the plant and the launch load power spectral densities, a disturbance analysis can be performed to determine the stresses in the mirror subject to the prescribed disturbances. The analysis used

is frequency domain, steady state, dynamic disturbance analysis. To begin, the integrated state-space model (Equation 3) is transformed into a frequency domain transfer function matrix as follows:

$$G_{zw} = C_z(sI - A)^{-1}B_w \tag{24}$$

The PSD of the output can then be found using:

$$S_{zz} = G_{zw} \cdot S_{ww} \cdot G_{zw}^H \tag{25}$$

where S_{zz} is the PSD of the output, S_{ww} is the PSD of the disturbance input (Figures 8 and 11), G_{zw} is the system transfer function matrix (Equation 24), and ^{H} is the hermitian operator. The mean squared value of the outputs can then be found:[13]

$$\bar{z_i^2} = \frac{1}{2\pi}\int_{-\infty}^{+\infty} S_{zz}(j\omega)_{i,i}d\omega = \frac{1}{\pi}\int_{0}^{+\infty} S_{zz}(j\omega)_{i,i}d\omega \tag{26}$$

The square root of $\bar{z_i^2}$ yields the root-mean-square value of the output.

In this model, the outputs, $\sqrt{\bar{z_i^2}}$, are in plane stresses for the selected elements. Each element has three associated stresses: σ_{xx}, σ_{yy}, and σ_{xy}. However, these stresses are in the local coordinate systems of the elements, as defined by the projection transformation described in Section 4.1.1. Therefore, to compare stresses across the mirror, the three local coordinate stresses are transformed to principle and von-mises stresses.[7]

$$\sigma_{p1} = \frac{\sigma_x + \sigma_y}{2} + \sqrt{\frac{\sigma_x - \sigma_y}{2} + \sigma_{xy}^2} \tag{27a}$$

$$\sigma_{p1} = \frac{\sigma_x + \sigma_y}{2} - \sqrt{\frac{\sigma_x - \sigma_y}{2} + \sigma_{xy}^2} \tag{27b}$$

$$\sigma_{vm} = \sqrt{\frac{(\sigma_{p1} - \sigma_{p2})^2}{2} + \frac{\sigma_{p1}^2}{2} + \frac{\sigma_{p2}^2}{2}} \tag{27c}$$

The von-mises stresses can then be compared element by element to determine the maximum stress in the system.

This completes the modeling process for using dynamic, state-space techniques to analyze launch stresses in mirrors. This process takes the mirror design parameters and desired disturbance spectrum and uses them to compute the stresses in any chosen element.

7. CONCLUSIONS AND FUTURE WORK

This paper describes a process for evaluating the stresses in mirrors through the use of state-space and frequency domain analysis techniques. All aspects of the model are parametrically defined, making it easy to analyze varying designs. The first step is the finite element model. The model here includes a lightweight, rib-stiffened, actuated, hexagonal mirror segment and kinematic bipod supports. The geometry, grid points, elements, and material properties are all defined based on the parametric inputs. With the FEM definition, NASTRAN solves the FEA to determine the frequencies and mode shapes, which are then used to define the system dynamics in a state-space model. Subsequently, interpolation functions and FEM theory are used to transform the nodal displacement outputs from the model into stresses for the given element, and the model is transformed to accept an acceleration spectral density and a pressure spectral density. Next, the disturbance input PSDs are defined, and combined with the plant model to perform a frequency domain dynamic disturbance analysis. Finally, the stresses in local, elemental coordinates are transformed to principle stresses and von mises stresses that can be compared across the mirror and analyzed for launch survival.

The methodology presented above can be very useful for mirror design and analysis. It will allow for rapid trade space generation of differing mirrors undergoing launch disturbances. This will allow for determination of limitations on areal density, rib structure, and other basic design variables. This will be extremely useful in the design of future mirrors, especially as the apertures continue to grow and the areal densities and masses continue to decrease. Additionally, there will be a point at which the mirrors no longer survive the harsh launch environment. The benefit of the dynamic analysis described above is that it allows for easy inclusion of both passive and active damping techniques. Passive and/or active damping will presumably allow more mirrors to survive the launch. However, the amount of additional damping necessary is design specific, and not all levels of damping will cost the same amount. Therefore, the parameterized model will continue to be used to include the various damping possibilities in order to get an accurate picture of the design landscape.

The design methodology described herein is a stepping stone to further design guidelines and mirror optimization. Future work includes validating all aspects of the current model and determining the reaction of current mirrors to launch. This will involve trade space exploration and optimization to find the best mirrors for launch survival, and to establish design variable limitations without any additional control or damping. Additionally, passive damping techniques will be examined, including isolation and shunted piezos. Finally, active damping will be pursued if necessary. This could be accomplished using the embedded piezoelectric actuators in the mirror, providing a damping solution with no additional hardware. In all cases, the goal is to determine the best mirrors for a given mission, and to extend the state-of-the-art in mirror design. This work will progress to hopefully eliminate launch survival as one of the major design drivers, and, instead, will present designs that are robust to launch.

REFERENCES

[1] Stahl, H. P. and Feinberg, L., "Summary of nasa advanced telescope and observatory capability roadmap," *Aerospace Conference, 2007 IEEE* , 1–11 (3-10 March 2007).

[2] Beckwith, S. V. W., "Space telescopes after the james webb space telescope," in [*Proceedings of SPIE: UV/Optical/IR Space Telescopes: Innovative Technologies and Concepts*], **5166**, 1–7, SPIE (2004).

[3] Ealey, M. A., "Fully active telescope," in [*UV/Optical/IR Space Telescopes: Innovative Technologies and Concepts*], MacEwen, H. A., ed., **5166**, 19–26, SPIE (2004).

[4] MacEwen, H. A., "Separation of functions as an approach to development of large space telescope mirrors," in [*Proceedings of SPIE: UV/Optical/IR Space Telescopes: Innovative Technologies and Concepts*], **5166**, 39–48, SPIE (2004).

[5] Uebelhart, S. A., Cohan, L. E., and Miller, D. W., "Design exploration for a modular optical space telescope architecture using parameterized integrated models," in [47^{th} *AIAA/ASME/ASCE/AHS/ASC Structures, Structural Dynamics & Materials Conference*], (May 1-4, 2006). AIAA 2006-2083.

[6] Bathe, K.-J., [*Finite Element Procedures*], Prentice-Hall (1996).

[7] Gere, J. M., [*Mechanics of Materials*], Brooks/Cole, 5 ed. (2001).

[8] Nigam, N. C. and Narayanan, S., [*Applications of Random Vibrations*], Narosa Publishing House (1994).

[9] Tedesco, J. W., McDougal, W. G., and Ross, C. A., [*Structural Dynamics Theory and Applications*], Addison-Wesley (1999).

[10] "Power extension package (pep) system definition extension, orbital service module systems analysis study, volume 5: Environmental specification," tech. rep., NASA (August 1979). NASA-CR-160325.

[11] Wertz, J. R. and Larson, W. J., [*Space Mission Analysis and Design*], Microcosm, Inc, Torrance, CA, Kluwer Academic Publishers, Boston, 3^{rd} ed. (1999).

[12] Sarafin, T. P., ed., [*Spacecraft Structures and Mechanisms - From Concept to Launch*], Microcosm, Inc. and Kluwer Academic Publishers (1995).

[13] Brown, R. G. and Hwang, P. Y. C., [*Introduction to Random Signals and Applied Kalman Filtering*], John Wiley and Sons, 3rd ed. (1997).